BRL-TR-3357

(2)

TECHNICAL REPORT BRL-TR-3357

BRL

A MECHANISM FOR THE PHOTODISSOCIATION OF CARBON MONOXIDE AT 193 nm

BRAD E. FORCH
U.S. ARMY BALLISTIC RESEARCH LABORATORY

CLIFTON N. MERROW
U.S. ARMY CHEMICAL RESEARCH, DEVELOPMENT, AND ENGINEERING CENTER

JUNE 1992

U.S. ARMY LABORATORY COMMAND

BALLISTIC RESEARCH LABORATORY
ABERDEEN PROVING GROUND, MARYLAND

NOTICES

Destroy this report when it is no longer needed. DO NOT return it to the originator.

Additional copies of this report may be obtained from the National Technical Information Service, U.S. Department of Commerce, 5285 Port Royal Road, Springfield, VA 22161.

The findings of this report are not to be construed as an official Department of the Army position, unless so designated by other authorized documents.

The use of trade names or manufacturers' names in this report does not constitute indorsement of any commercial product.

REPORT DOCUMENTATION PAGE

Form Approved
OMB No. 0704-0188

1. AGENCY USE ONLY (Leave blank)	2. REPORT DATE	3. REPORT TYPE AND DATES COVERED
	June 1992	Final, January 91–June 91

4. TITLE AND SUBTITLE
A Mechanism for the Photodissociation of Carbon Monoxide at 193 nm

5. FUNDING NUMBERS
PR: 1L161102AH43

6. AUTHOR(S)
Brad E. Forch and Clifton N. Merrow*

7. PERFORMING ORGANIZATION NAME(S) AND ADDRESS(ES)

8. PERFORMING ORGANIZATION REPORT NUMBER

9. SPONSORING / MONITORING AGENCY NAME(S) AND ADDRESS(ES)
U.S. Army Ballistic Research Laboratory
ATTN: SLCBR-DD-T
Aberdeen Proving Ground, MD 21005-5066

10. SPONSORING / MONITORING AGENCY REPORT NUMBER
BRL-TR-3357

11. SUPPLEMENTARY NOTES
*Mr. Merrow works at the U.S. Army Chemical Research, Development, and Engineering Center, Aberdeen Proving Ground, MD

12a. DISTRIBUTION / AVAILABILITY STATEMENT
Approved for public release; distribution is unlimited.

12b. DISTRIBUTION CODE

13. ABSTRACT *(Maximum 200 words)*

The photodissociation of carbon monoxide at 193 nm has been investigated using resonance enhanced multiphoton ionization detection of atomic oxygen and carbon fragments. The results of these experiments indicate a quadratic photodissociation process in CO at 12.8 eV. In addition, the nascent fine structure branching ratios of atomic oxygen $2p^4$ ($^3P_{2,1,0}$) produced in the 193-nm photodissociation of CO are reported using both multiphoton laser-induced fluorescence and ionization detection. Analysis of the experimental data and computer-generated simulations indicate that the distributions are not statistical.

14. SUBJECT TERMS
carbon monoxide, photodissociation, oxygen atoms

15. NUMBER OF PAGES
36

16. PRICE CODE

17. SECURITY CLASSIFICATION OF REPORT	18. SECURITY CLASSIFICATION OF THIS PAGE	19. SECURITY CLASSIFICATION OF ABSTRACT	20. LIMITATION OF ABSTRACT
UNCLASSIFIED	UNCLASSIFIED	UNCLASSIFIED	UL

INTENTIONALLY LEFT BLANK.

TABLE OF CONTENTS

INTENTIONALLY LEFT BLANK.

LIST OF FIGURES

INTENTIONALLY LEFT BLANK.

ACKNOWLEDGMENTS

This work was supported in part by the Air Force Office of Scientific Research (AFOSR) and the U.S. Army Ballistic Research Laboratory. Purchase of data acquisition and processing equipment through the Productivity Capital Investment Program (PCIP) is gratefully acknowledged. Helpful discussions with Drs. W. Anderson, M. McQuaid, and D. Dayton are appreciated.

INTENTIONALLY LEFT BLANK.

1. INTRODUCTION

The dissociation processes of high-lying electronic states of carbon monoxide (CO) have been the subject of numerous theoretical (Cooper and Langhoff 1981; O'Neil and Schaefer 1970; Fock, Gurtler, and Koch 1980; Cooper and Kirby 1981; Letzelter et al. 1987; Vidal 1988; and Sekine, Adachi, and Hirose 1989) and experimental (Bokor, Zavelovich, and Rhodes 1980; Sausa, Alfano, and Miziolek 1987; Meijer et al. 1988; Laufer, McKenzie, and Huo 1988; Hill et al. 1990; and Merrow and Forch 1990) investigations. Experimental work on the photodissociation of CO have frequently utilized the argon fluoride (ArF) excimer laser because of several important reasons. The ArF excimer laser operates at 193 nm in the ultraviolet; therefore, it is a convenient source of high energy photons (6.4 eV). Also, since the absorption of two 193-nm photons (6.4 eV each) just exceeds the dissociation energy (Huber and Herzberg 1979) [D_0 (C-O) = 11.09 eV] from the ground electronic state CO ($X^1\Sigma$), it is well suited for photodissociation experiments. Although the photodissociation mechanism of CO and the states involved near 12.8 eV is not entirely understood at present, recent experimental and theoretical work has given new insight into the photodissociation processes. In particular, the work of Hill et al. (1990) suggests that the interaction between the CO $^3\Pi$ Rydberg and $^3\Pi$ valence states near 12.8 eV induces dissociation on a picosecond, or faster, time scale. They have also shown that two-photon dissociation of CO completely dominates over processes such as multiphoton ionization and higher order dissociation processes at laser power densities up to 30 GW/cm^2.

Recent work in our laboratory also suggests a two-photon dissociation process in CO at 193 nm (Merrow and Forch 1990). Unlike previous experiments which used a single laser for both the photodissociation of CO and for the detection of atomic carbon photofragments, we devised a two-laser experiment to probe the photodissociation using oxygen atom two-photon laser-induced fluorescence. We showed that 193-nm photodissociation of CO produced atomic oxygen in three ground electronic spin-orbit split states, oxygen $2p^4(^3P_{2,1,0})$. Two-photon excitation of the oxygen $2p^4(^3P_{2,1,0})\rightarrow 2p^3 3p(^3P_{2,1,0})$ transitions near 225.6 nm (see Figure 1) and fluorescence detection at 844.7 nm following the 193-nm photodissociation yielded a near quadratic photolysis laser power dependence ($n = 1.90 \pm 0.09$). A simple dissociation mechanism was proposed wherein single-photon absorption at 193 nm produces CO ($a^3\Pi$, $u' = 2$), then the subsequent absorption of an additional ArF photon to a state with suspected triplet character leads to rapid dissociation. The present experimental study was undertaken to further investigate the 193-nm dissociation of CO.

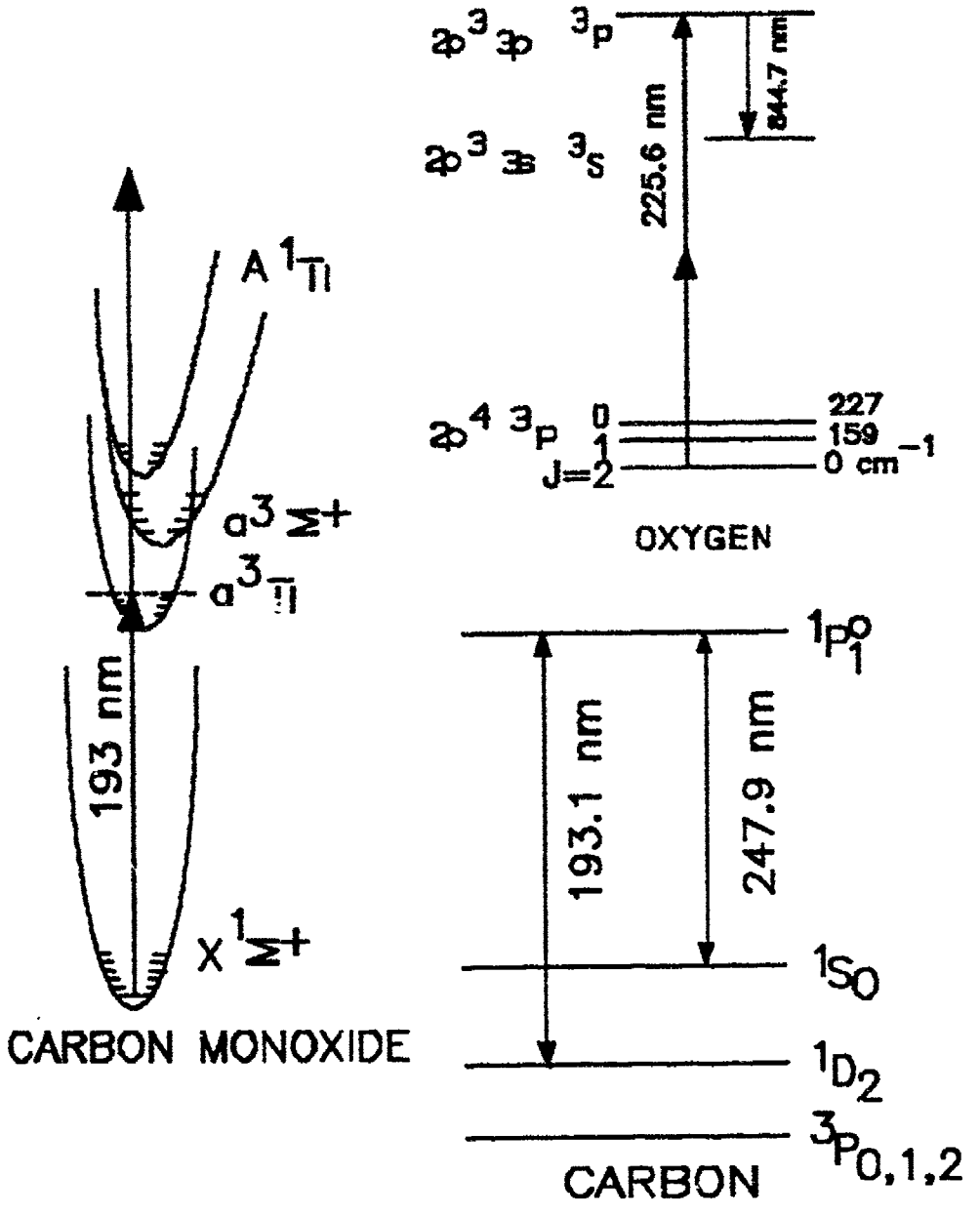

Figure 1. Simple Energy Level Diagrams for Carbon Monoxide, Atomic Oxygen, and Atomic Carbon.

Our initial experimental measurements were made in a very simple low pressure flow cell which was operated in the millitorr pressure range. These investigations have been extended into a high vacuum ($\sim 10^{-7}$ torr) pulsed molecular beam apparatus which is equipped with a time-of-flight mass spectrometer (TOFMS). This new experimental setup allows for both mass selection and ionization detection using a pump-probe laser configuration. Subsequent to ArF laser photodissociation of CO, ions of atomic oxygen and atomic carbon are selectively detected using (2+1) and (1+1) Resonance Enhanced Multiphoton Ionization (REMPI), respectively. A two-photon dissociation process in CO at 193-nm is reported using both REMPI detection schemes, which is in excellent agreement with our previous results (which used multiphoton laser-induced fluorescence). In addition, we report the nascent fine structure branching ratios of atomic oxygen $2p^4$ ($^3P_{2,1,0}$) from 193-nm photodissociation of CO using both REMPI detection and multiphoton laser-induced fluorescence detection. These results indicate that the distribution that was measured is not statistical. Computer-generated simulations of the experimental excitation spectra were made and yield a distribution which would correspond to a thermal temperature of 1,100 ±200 K.

2. EXPERIMENTAL

A schematic of the apparatus used for these experiments is shown in Figure 2 and has been previously outlined (Merrow and Forch 1990). A brief description of the new instrumentation and experimental procedure is as follows. A pulsed molecular beam of neat carbon monoxide (Matheson UHP Grade) was generated using an R. M. Jordan pulsed molecular valve system (Lubman and Jordan 1985). The beam pulse duration (~30 μs) was measured with a fast ion gauge which could be positioned to intersect the beam for measurement and be removed as required. The molecular beam was skimmed (500-μm skimmer, Beam Dynamics) and passed into a differential pumped region of the TOFMS, which was maintained at a pressure of $\sim 10^{-7}$ torr. The CO beam was photolyzed with the output of a loosely focused (1,000-mm focal length lens) broad-band ArF excimer laser (Lumonics model No. 440) at low laser energy density (<0.01 GW/cm^2/cm^{-1}). The photolysis laser beam was contained in a windowed tube which was flushed with N_2 or He to avoid its attenuation by molecular oxygen absorption via the Schumann-Runge bands (Yoshino, Freeman, and Parkinson 1984). A cryogenic gas processor was attached to the ArF laser to extend the gas fill life. Photo-produced ground electronic state oxygen $2p^4(^3P_{2,1,0})$ atoms were detected using (2+1) REMPI near 225.6 nm[16] from the probe laser (Nd:YAG/dye/wavelength extension system, Quanta Ray model No. DCR-2A, No. PDL-1, and No. WEX-1). Photo-produced atomic carbon $2p^2(^1D_2)$ atoms were detected using (1+1) REMPI near 247.9 nm. The ions were accelerated in the TOFMS by three grid plates each separated by 10 mm.

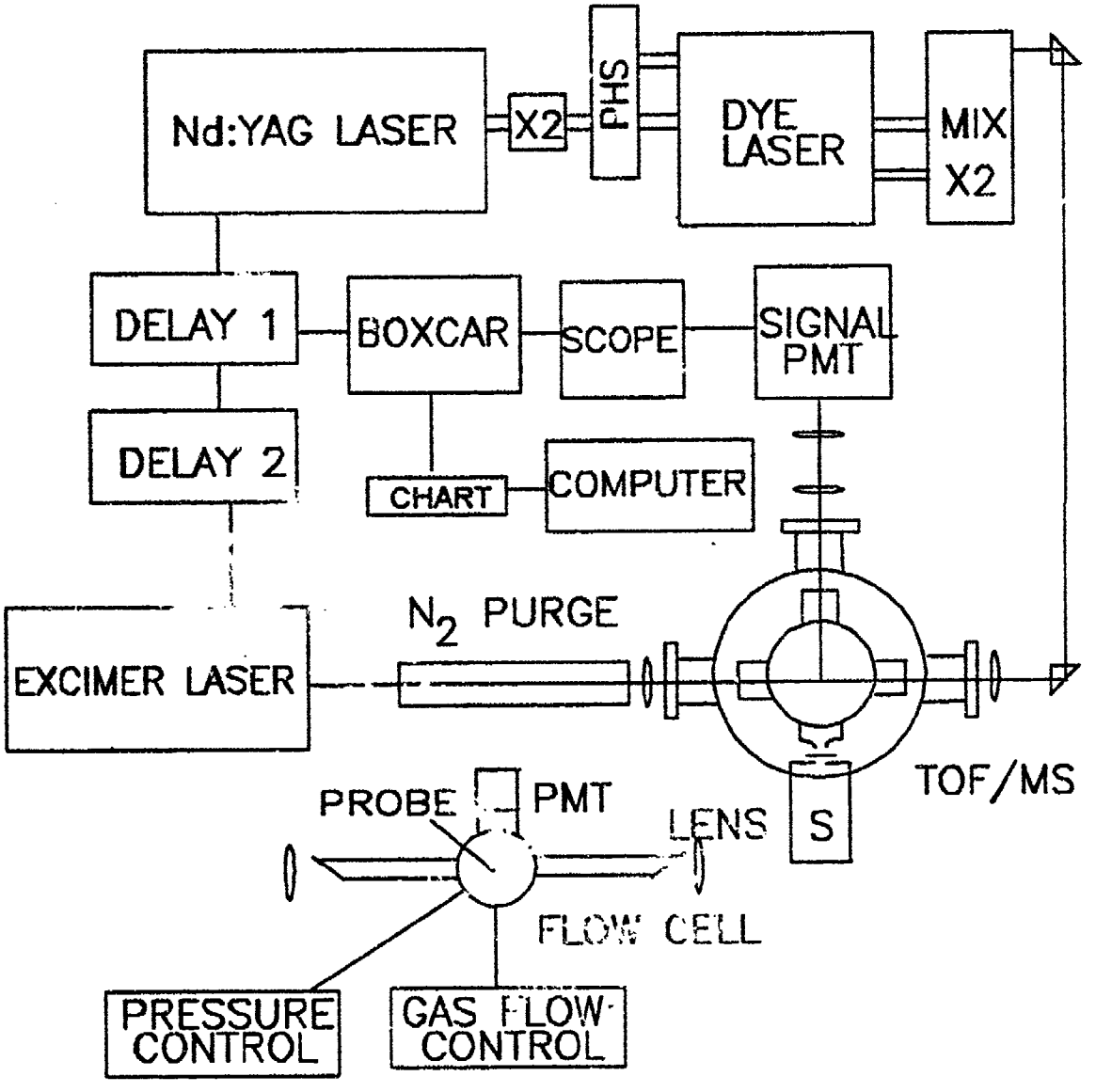

Figure 2. Schematic of Experimental Apparatus.

The ions are repelled by a plate biased at +2,300 V, drawn through an extraction grid biased at 1,900 V and then they are accelerated through the ground grid into the flight tube. The differentially pumped region is enclosed in a vertical liquid nitrogen trap which minimizes background gas contamination and is a factor of nearly 100 times lower pressure than the preskimmed chamber region (10^{-5} torr) which is backed by a 10-in oil diffusion pump. Essentially very little hydrocarbon background was observed using a polyphenyl ether diffusion pump fluid (Santovac 5) with low vapor pressure ($\sim 10^{-10}$). The diffusion pump is separated from the main chamber by a gate valve and liquid nitrogen-cooled trap and baffle, which eliminates oil backstreaming. The drift tube region is approximately 146 cm long and is backed by a 6-in turbomolecular pump. The ion detector is a dual-channel plate which provides a gain of 10^7 and is terminated into a 50-Ω connector. The rise time of the detector is very fast (subnanosecond), and a grid is located in front of the detector, which ensures that the drift region in the flight tube is field free (since the front surface of the device is operated at a high negative potential [3,000 V] [Lubman and Jordan 1985]). The ion beam can be steered to the detector grid with four X-Y deflector plates located along the drift tube which compensate for the traverse displacement due to the initial beam velocity vector. The time synchronization of the pulsed valve, photolysis laser, and probe laser were controlled with precision digital pulse-delay generators (Stanford Research Systems, model No. DG 535). The Nd:YAG oscillator sync-out pulse triggered the pulse valve and the pulse-delay generator. An output trigger pulse from the delay generator was then used to fire the excimer laser with a selectable delay prior to the probe laser beam. Ion signals were detected with a 500-MHz digital scope to the probe laser beam. Ion signals were detected with a 500-MHz digital scope (Hewlett-Packard model No. 54111D) and/or boxcar integrator-computer system.

3. RESULTS AND DISCUSSION

3.1 System Calibration. Since our intention in this work was not only to investigate the photodissociation of CO using oxygen atom (2+1) REMPI and carbon atom (1+1) REMPI but to also measure the nascent ground electronic spin orbit split state distribution of photolytically produced oxygen $2p^4(^3P_{2,1,0})$, experiments were performed to ensure that such a distribution could be measured with our experimental setup. In addition, the measurement of nascent product state populations under collision-free conditions using both ionization and fluorescence detection as a comparison aids in the establishment of the validity of the measurements. In particular, it is desirable that the probe laser output energy remain constant (flat) in the scan wavelength region 225–227 nm because of the nonlinear nature of the multiphoton excitation scheme used for the detection of atomic oxygen. This required tuning of the dye

laser composition and concentration until the frequency doubled and mixed output in this region was uniform. First, we made up oscillator and amplifier laser-dye solutions which were a mixture of Rhodamine 590 and Rhodamine 610. The output laser energy was measured in the wavelength region 225–226 nm, then the laser-dye solution concentrations were changed by injecting microliter quantities of a saturated dye solution of Rhodamine 610 until the output energy was constant over this scan range. We found that after continuous operation of the laser system for 3 hours, the output energy was skewed ~10% toward the blue. Therefore, no dye solution was used more than 2 or 3 hours in the course of this work without changing or adding more saturated Rhodamine 610 solution. The approximate dye concentrations of the oscillator and amplifier stages were 2.2×10^{-4} M and 3.2×10^{-5} M, respectively, with a composition of 69% Rhodamine 590 and 31% Rhodamine 610.

Reliable distribution ratios and laser power dependencies could be measured without the need for external calibration when both the photolysis and probe laser systems were optimized to reduce saturation effects. Excitation spectra of the thermalized oxygen atom ground electronic fine structure produced in CO photolysis was recorded in N_2 or Ar buffer gas at a total pressure of ~80 torr. A computer code was written to simulate the spectrum and fit the distribution to a thermodynamic temperature. A simple Gaussian-type function of full width at half maximum (FWHM) of ~1 cm^{-1} was found to closely represent the spectral profile of the laser excitation source near 225.6 nm since the signals in Figure 3a are much broader than the O-atom doppler width and are primarily determined by the laser line width (Bischel, Perry, and Crosley 1984). The fine structure splittings of the oxygen $2p^3\ 3p\ ^3P_j$ levels in the upper state are < 0.5 cm^{-1} and are therefore not resolved with our resolution, so only single peaks were observed. Using this simple model, the experimental data were fit to a Boltzman distribution with a thermodynamic temperature of 309 ±30 K (Figure 3b), which is very close to the expected room temperature result. All of the raw data were digitized and normalized to the intensity of the $2p^4(^3P_0)$ fine structure component. Fluorescence power dependence measurements were also made to ensure that the probe laser two-photon excitation process was not saturated and was indeed quadratic. The combined results of the experiments and simulations indicate that the distributions we measure are reliable.

The TOFMS was time-to-mass calibrated using a pulsed molecular beam of hydrogen. There are two-photon resonant transitions from the four lowest rotational states of H_2 (Q lines of the [2,0] bank of the EF-X system) that coincidentally fall within the gain of the free-running ArF laser near 193 nm. H^+ and H_2^+ are produced from multiphoton dissociation of H_2 and (2+1) REMPI of H_2, respectively, using the intermediate E,F excited electronic state as described by Buck, Parker, and Chandler (1988). Single-

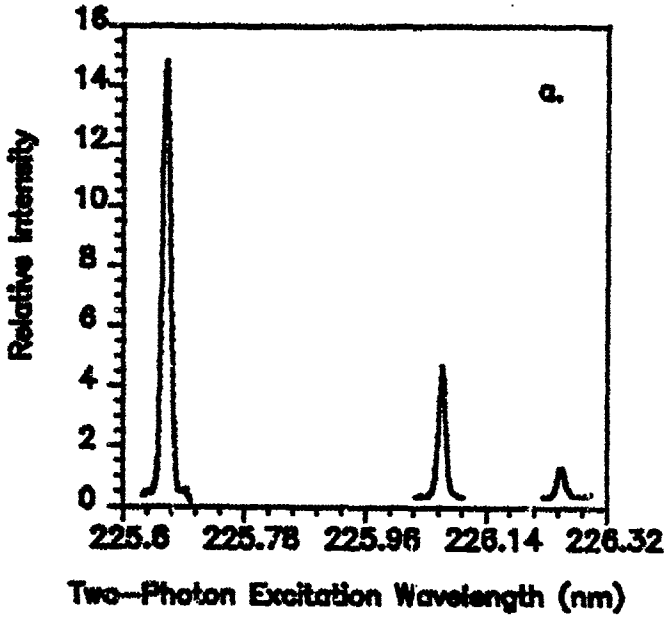

Figure 3a. Thermalized Two-Photon Laser-Induced Fluorescence Excitation Spectrum of Atomic Oxygen.

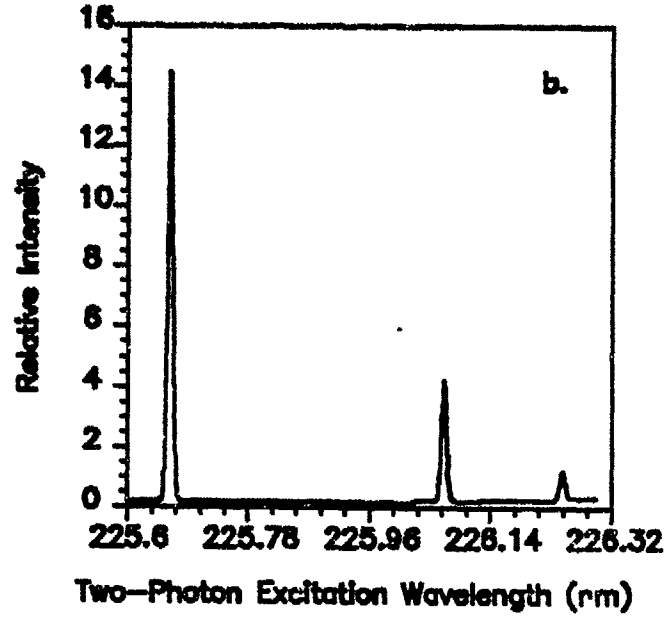

Figure 3b. Computer-Generated Excitation Spectrum of the Data in Figure 3a.

laser photolysis of H_2 at 192 nm produced two ion signals at 2.37 μs and 3.35 μs, respectively, relative to the laser light pulse signal which triggered the scope. These flight times correspond to the arrival of H^+ and H_2^+ at the detector. A simple computer program was then written which calculates trajectory flight times based upon the accelerating voltages on the grid plates, drift tube length, and other parameters particular to our TOFMS. The calculated flight times (2.3689 μs and 3.3502 μs for H^+ and H_2^+) are in excellent agreement with the experimentally observed values.

We then began experimental measurements on the photodissociation of CO in the TOFMS. These experiments require the temporal synchronization of three pulsed sources—the photolysis probe lasers, and molecular beam valve. The temporal jitter of the Nd:YAG-dye laser system is on the order of only several nanoseconds, and the jitter of the ArF photolysis laser can be reduced to ~2 ns by using a charge-on-demand triggering feature designed into the laser electronics. However, regardless of the triggering scheme used, there was an inherent jitter of ~ ±50 ns in the opening of the pulsed molecular beam relative to the trigger signal. The pulsed valve was operated under choked flow conditions wherein the flow is essentially conductance limited and has a square wave profile of 30 μs as measured with the fast ion gauge. Therefore, the pulse duration of the molecular beam, is at least two orders of magnitude wider than the laser pulses. We found that when the photolysis laser beam was overlapped within the center of the pulsed valve beam the effects of the temporal jitter were inconsequential. We also found that the high-conducting hairpin loop in the pulsed valve operator system required 30–40 min of conditioning (continuous operation) to ensure that the pulse width and intensity of the molecular beam were uniform with time. Experiments which produced a thermalized distribution of atomic oxygen in the TOFMS were also performed as a check of the atomic oxygen (2+1) REMPI detection procedure. The tungsten wire filament of the fast ionization gauge was biased at low current, then positioned in the path of the pulsed molecular beam. Thermal dissociation of some CO molecules which collided with the wire filament and grid produced ground state oxygen atoms. Ground electronic state hydrogen and deuterium atoms have been produced from beams of molecular hydrogen and deuterium using this technique as recently described by Downey and Hozack (1989). Laser power dependence measurements for the detection of these atoms gave a value $n = 2.73 \pm 0.28$, and computer simulation of the experimental excitation spectra gave a distribution with a temperature of 340 ±40 K. We observed that essentially no O^+ signal was generated by the filament from the thermal dissociation of CO when the applied current was very low. These results gave us confidence that the (2+1) REMPI detection scheme would allow for the determination of the photolysis laser power dependence for CO, yield reliable distributions, and that saturation effects were minimal at these low laser energy densities.

3.2 Atomic Oxygen (2+1) REMPI. The proposed photodissociation mechanism for CO at 193 nm is essentially a two-step process. The initial absorption of the first ArF photon from the ground electronic state of CO ($X^1\Sigma^+$) produces CO ($a^3\Pi$, $v = 2$), which subsequently absorbs one additional photon into a dissociative state with triplet character. Hill et al. (1990) have proposed that the interaction between $^3\Pi$ Rydberg and $^3\Pi$ valence states near 12.8 eV causes subnanosecond dissociation which precludes higher order processes. Therefore, minimal CO^+ signals should be observed from irradiation of CO at 193-nm. TOFMS were first recorded with only the 193 nm laser photolyzing the beam of CO. The laser energy density was ~0.01 GW/cm^2/cm^{-1}. Consistent with Hill et al. (1990) and our mechanism, we observed essentially no ionization signal from CO^+ above the background TOFMS noise at laser energy densities (~0.01 GW/cm^2/cm^{-1}), which were much lower than had been previously employed (Bokor, Zavelovich, and Rhodes 1980; Sausa, Alfano, and Miziolek 1981; Meijer et al. 1988; and Hill et al. 1990). However, an ion signal was observed which appeared at 8.2 μs, which has been assigned to C^+ and is consistent with the photoproduction of metastable carbon $2p^2(^1D_2)$ atoms, which were subsequently excited by an additional 193-nm photon to the carbon $2p3s(^1P_1)$ excited state and ionized by the absorption of another 193-nm photon. An ion signal which would have appeared at a delay of 9.5 μs relative to the photolysis laser pulse (for O^+) was not observed. It is also important to ensure that the probe laser beam was not inducing photolysis of CO under these conditions. Ion signals from neither CO^+ nor O^+ were observed when the laser tuned both on and off resonance of the three oxygen $2p^4(^3P_j)$ (2+1) REMPI transitions. Next, we began the pump-probe REMPI experiments.

Spatial overlap of the counterpropagating photolysis and probe laser beam was very difficult because of the limited viewing access into the differentially pumped region of the TOFMS. However, temporal synchronization of the two laser pulses was facilitated by viewing scattered laser light from a small orifice through which the colimated molecular beam exited (Figure 1). The initial delay between the photolysis and probe laser pulses was set at 40 ns. As the probe laser was scanned through the oxygen $2p^4(^3P_{2,1,0})\rightarrow 2p^3 3p(^3P_{2,1,0})$ transitions near 225.6 nm, O^+ ion signals appeared at 9.5 μs relative to the scope trigger signal from the probe laser. The apparatus was then tuned to maximize the signal output. The boxcar gate was fixed to mass select and integrate the O^+ signal as the probe laser was scanned and an excitation spectrum was recorded. A representative (2+1) REMPI spectrum is shown in Figure 4a. The same type of single-laser experiment was performed using only the probe laser beam which was tuned both on and off resonance of the three oxygen $2p^4(^3P_j)$(2+1) REMPI transitions and no ionization signals (neither CO^+, C^+, nor O^+) whatsoever were observed. This result indicates that under these experimental conditions, the probe laser beam was not inducing photolysis of CO. The spectrum was recorded in three

separate scans and the raw data was normalized to the intensity of the $2p^4(^3P_0)\rightarrow 2p^3 3p(^3P_{2,1,0})$ transition. Note that the relative ion signal intensities given in Figure 4a differ from those obtained in the thermalized distribution presented in Figure 3a and will be discussed shortly. Several power dependence measurements of the probe laser energy on the O^+ REMPI signals insured that the detection multiphoton process was not saturated. The slope (n) of an Ln-Ln plot of the O^+ intensity versus probe laser energy gives a near cubic dependence for the overall process ($n = 2.86 \pm 0.29$). In addition, laser power dependence measurements with the probe laser tuned to each of the three spin-orbit split states fell within these error bars. The non-integer value is due, in part, to experimental noise, pulse-to-pulse fluctuations in the laser output and partial saturation of the photoionization step which has a relatively larger photoionization cross section as compared to the two-photon absorption cross section in the first step of the (2+1) REMPI scheme (Bamford, Jusinski, and Bischel 1986).

We proceeded with the photolysis laser power dependence measurements. The majority of the photolysis laser power dependence measurements were performed with the probe laser tuned to the oxygen $2p^4(^3P_2)\rightarrow 2p^3 3p(^3P_{2,1,0})$ transitions because the signal intensity was largest there. A linear least-squares fit to the data gives a slope of $n = 1.78 \pm 0.28$ which indicates a quadratic dependence on the photolysis of CO. Quadratic dependencies of the photolysis laser on the dissociation were also observed with the probe laser tuned to detect O^+ at the excitation wavelengths for the other two oxygen atoms ground electronic spin orbit split states. A comparison of the results obtained using (2+1) REMPI ($n = 1.78 \pm 0.28$) with those obtained using oxygen-atom two-photon laser-induced fluorescence (Merrow and Forch 1990) ($n = 1.9 \pm 0.09$) are in good agreement.

Numerous control experiments serve as a critical check of the data and show that the oxygen atoms were not produced in a collisional process or by chemical reaction. We found that the oxygen atom signals increased linearly with pressure over an order of magnitude of pressure change. A quadratic dependence of the photolysis laser on CO was observed when the pump-probe delay time was varied from 50 ns to 500 ns. We also photolyzed CO outside the differentially pumped region in front of the skimmer to provide a much longer delay between the pump and probe laser beams. The spatial distance between the tip of the skimmer cone and the center of the ionization region is approximately 5 cm, and at beam velocities of $\sim 10^4$ cm/s the pump probe delay time is 500 μs. A photolysis laser power dependence of 1.71 ± 0.43 was determined. However, in the TOFMS, it is difficult to vary the pressure substantially since the operating pressure should be kept $< 10^{-6}$ torr to avoid arcing between the microchannel detector plates (which greatly reduces its operating lifetime) (Lubman and Jordan 1985). We also noted that when the

backing pressure of CO supplied to the pulsed valve is varied, then the linear velocity of the molecular beam changes and alters the time synchronization of the valve relative to the pump and probe lasers. Nonetheless, we performed experiments where the CO pressure was increased to allow the chamber pressure to reach near 10^{-5} torr, and a linear dependence of the O^+ signal on pressure was observed pressure range. The oxygen (2+1) REMPI signal was also found to vary linearly with CO pressure (10^{-7}–10^{-5} torr). However, owing to erratic behavior of the microchannel plate detector (noise spikes which occurred at the higher pressure range), these types of experiments were not pursued further.

3.3 Atomic Carbon (1+1) REMPI. An alternate approach to investigate the photodissociation is to detect atomic carbon in a pump-probe laser experiment. Since the photolysis of CO at 193 nm also produces metastable carbon $2p^2(^1D_2)$ atoms (Bokor, Zavelovich, and Rhodes 1980; Sausa, Alfano, and Miziolek 1987; and Hill et al. 1990), carbon atom (1+1) REMPI near 247.9 nm can be employed to investigate the dissociation. A 193-nm photolysis laser also excites the carbon $2p^2(^1D_2)\rightarrow 2p3s(^1P_1)$ transition at 193.1 nm, which radiates at 247.9-nm carbon $2p3s(^1P_1)\rightarrow 2p^2(^1S_0)$. The carbon $2p^2(^1S_0)$ atoms were then detected by pumping the reverse transition, carbon $2p^2(^1S_0)\rightarrow 2p3s(^1P_1)$, then photoionizing from the carbon $2p3s(^1P_1)$ state, (1+1) REMPI. Carbon ions which were produced from the 193-nm photolysis laser could easily be separated from those produced by the 247.9-nm probe laser with a time delay. For example, if the time delay between the photolysis and probe lasers was set at 20 ns, then carbon ions which were produced by the probe laser (although less intense) appeared as separate peaks, delayed 20 ns in the TOFMS signal with ions produced by the photolysis laser. Laser power dependence measurements for the probe laser detection of C^+ were made at several photolysis laser energies (0.1–0.6 mJ) and gave a value n = 1.74 ±0.39 for the (1+1) REMPI process. Neither C^+ nor CO^+ signals were observed when the probe laser alone was fired (~0.1 mJ). A photolysis laser power dependence of 1.61 ±0.37 was measured, which falls within the error bars of the uncertainties of the measurements using the other detection procedures.

3.4 Atomic Oxygen Nascent State Distributions. As mentioned earlier, the relative intensities of the O^+ signals differ from those recorded in a thermalizing bath of inert buffer gas, refer again to Figures 3a and 4a. A computer simulation of the spectrum is given in Figure 4b and yields a distribution ratio $^3P_2$:$^3P_1$:$^3P_0$ = 0.61:0.30:0.09, which would correspond to a thermalized Boltzman temperature of 1,100 ±200K. Furthermore, the relative distribution ratios we obtained using oxygen atom (2+1) REMPI is similar to the distribution ratios we obtained using oxygen atom two-photon laser-induced fluorescence in a flow cell (Merrow and Forch 1990). Apparently, the nascent state distribution we measured using

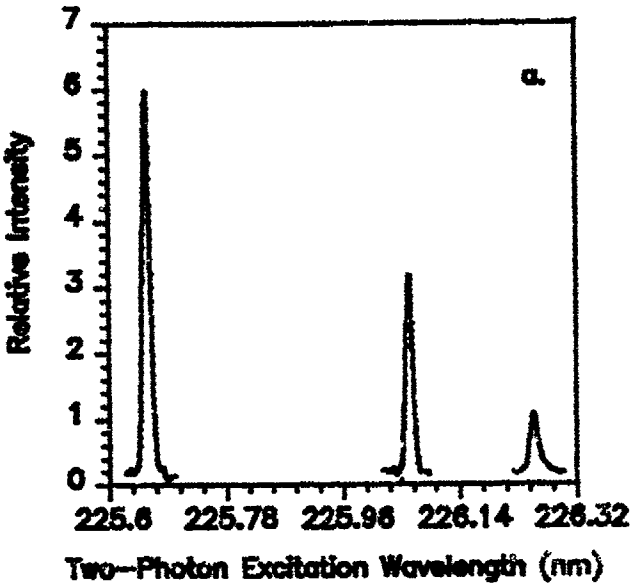

Figure 4a. (2+1) REMPI Excitation Spectrum of Atomic Oxygen.

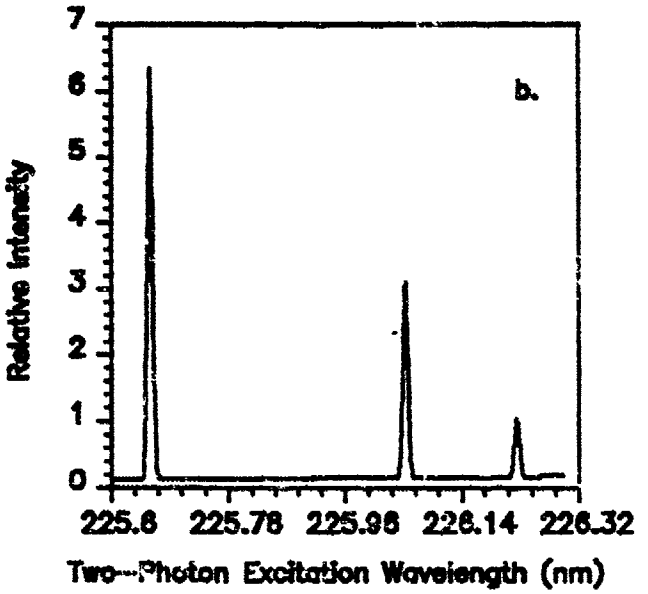

Figure 4b. Computer-Generated Excitation Spectrum Fit to a Thermodynamic Temperature of 1,000 ±200K.

either detection technique not statistical. We found that in a collisionless environment (10^{-7} torr), the relative distribution ratios did not change with delay time (up to 500 ns). The distributions were insensitive to pressure change in the range of 10^{-5}–10^{-7} torr and were, therefore, unperturbed by collisional relaxation processes. To our best knowledge, this is the first report of the fine structure branching ratios of atomic oxygen in the 193-nm photodissociation of CO.

Information on the nature and possible identity of predissociating states may be revealed by the spectroscopy of the photofragments and the product states into which they are produced. Complications may arise when any number of crossing potentials are involved in the dissociation, particularly at intermediate internuclear separations, and affect product state distribution channels and fine structure distributions. In turn, knowledge of the fragment fine structure distributions may discern, in part, the nature of the potentials involved in the predissociation (Lee and Freed 1987). For example, recent results of Huang and Gordon (1990) on the multiplet state distribution of $2p^4$ ($^3P_{2,1,0}$) produced in the 193-nm photodissociation of SO_2 gives the first report of the statistical distribution of atomic multiplet states in a photodissociation reaction. This distribution corresponds to the degeneracy weightings of the high temperature limit, 5:3:1. A statistical distribution of multiplet states is expected in a sudden "mapping" (Lee and Freed 1987; Huang and Gordon, to be published) of close lying fine structure states excited by the photon onto the asymptotic states of the fragments. For a direct dissociation, the populations are proportional to the multiplet degeneracies. Highly nonstatistical distributions may result from a "slow" dissociation. Huang and Gordon (to be published) give strong evidence that to the contrary, the dissociation is slow, and oxygen $2p^4$ ($^3P_{2,1,0}$) states are produced only through predissociation; therefore, exit channel mixing effects are responsible for the statistical distribution. Furthermore, Huang and Gordon (to be published) and Matsumi and Kawasaki (1990) report that in photodissociation at 157 nm, the population of the ground state (J = 2) was found to predominate from dissociation from the B $^3\Sigma_u$ state.

Experiment and calculation show that a room temperature distribution of atomic oxygen yields a population ratio $^3P_2$:$^3P_1$:$^3P_0$ = 0.74:0.21:0.05, and in the high temperature limit, the relative distribution will yield a population ratio $^3P_2$:$^3P_1$:$^3P_0$ = 5:3:1, which corresponds to the statistical weighting factor of the multiplet degeneracies (2J+1). It is noteworthy that the relative distribution ratios rapidly converge near 2,500 K to a distribution which has already approached the near high temperature limit (Figure 5). For example, the observation of atomic oxygen ground state splittings in combustion media where the adiabatic flame temperature is on the order of 2,500 K gives distributions which cannot be readily distinguished

from the high temperature limit. In our measurement of the nascent spin-orbit populations, the distribution is colder than the high temperature limit.

Kinetic energy analysis of the photofragments (Hill et al. 1990) and the absence of molecular ion fragments (CO^+) suggest predissociative lifetimes of picoseconds or less. In the case of CO photodissociation in the region of 12.8 eV, there are several Rydberg states of the proper symmetry for two-photon excitation from the CO ($X^1\Sigma^1$) ground electronic state (Bokor, Zavelovich, and Rhodes 1980). This energy is ~0.44 eV above the dissociation pathway which correlates to the production of metastable carbon $2p^2(^1D_2)$ and oxygen $2p^4(^3P_{2,1,0})$ (Krupenie 1966) states, which have been measured. If oxygen $2p^4$ ($^3P_{2,1,0}$) is left with a kinetic energy of ~0.21 eV (Hill et al. 1990), then this would yield a temperature of 1,600 K when fitted to a Boltzman distribution, which is close to our measurement. Although the exact nature of the state(s) reached is not entirely certain, two-photon excitation to the $c^3\Pi$ Rydberg state which is predissociated by $^3\Pi$ valence states (Hill et al. 1990) would yield the final product states which we have observed.

Two-photon excitation of CO may leave the molecule in a dissociative continuum which correlates to carbon $2p^2(^1D_2)$ and oxygen $2p^4(^3P_{2,1,0})$, or the excitation may terminate in discrete vibronic Rydberg states which are predissociative and yield these same product states. The observation of a resonance in the dissociation yield from a discrete excited state vibrational level would aid in the identification of the predissociative level and understanding of the dynamics. Here, it is important to mention that the spectral line width of the free-running ArF laser used in this work is ~150 cm^{-1} FWHM, and it excites a manifold of rotational lines in the CO ($a^3\Pi$, $v = 2$) level one-photon transitions. The resonances which have been observed in the dissociation are those which arise in transitions from the CO ($a^3\Pi$, $v = 2$) level (Meijer et al. 1988; Hill et al. 1990). Single-photon dissociation from this envelope of rotational levels yields the distribution of atomic oxygen spin-orbit states that we have measured over all of these levels. A tunable excimer laser with a much narrower bandwidth can resolve single rotational transitions from $J = 6$ to $J = 26$ in the electronic and vibrational ground state of CO perhaps also reveal Coriolis rotational effects which may influence the nascent oxygen spin-orbit distributions, which may be particularly prominent at higher J levels. Theoretical calculations (on OH dissociation) further show that nonadiabatic couplings influence the oxygen atom fine structure branching ratios and increase as a function of the J quantum number because of Coriolis coupling with J (Lee and Freed 1987). It has been shown (Hill et al. 1990) that dissociative processes which do produce C and C^+ exhibit a resonance effect which originates in the CO ($a^3\Pi$, $v = 2$) level; however, the CO^+ yield is essentially negligible and does not

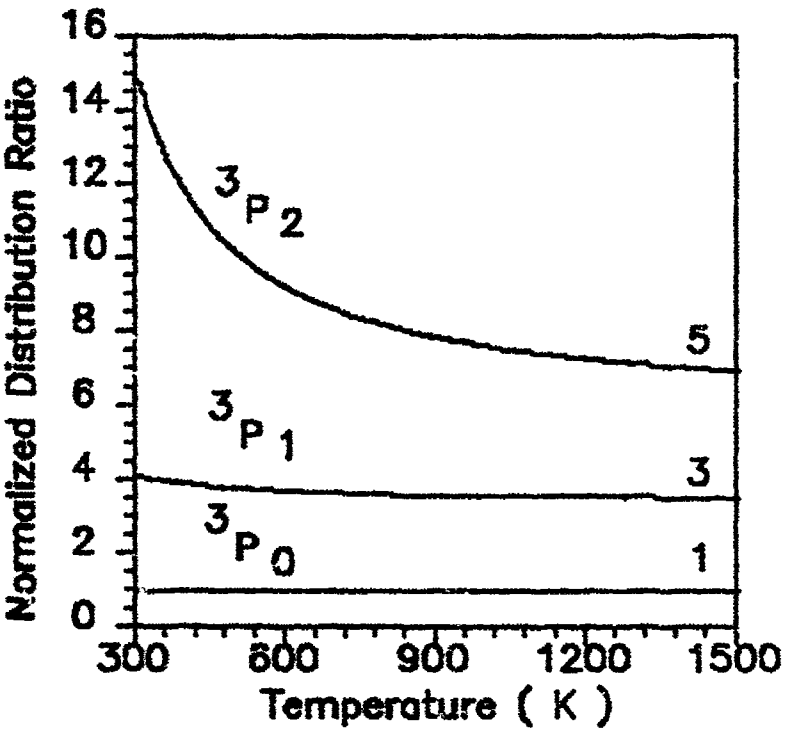

Figure 5. Calculated Distribution Ratios of Atomic Oxygen $2p^4(^3P_{2,1,0})$ Plotted vs. Temperature.

exhibit this frequency dependence. Similar experimental measurements using a tunable excimer laser to measure the frequency dependence of the yields of atomic oxygen in CO photodissociation which originate in the CO ($a^3\pi$, $v = 2$) level have not yet been performed to our best knowledge.

We thought that perhaps we could obtain information on rotational effects on the spin-orbit distributions by cooling ground electronic state CO ($X^1\Sigma^1$) in a supersonic expansion. Modulation of rotational populations of ground state molecules that are excited into higher lying electronic states have shown differing dynamical behavior using this simple technique, which has been attributed to Coriolis coupling (Saigusa, Forch, and Lim 1983; Forch and Lim 1984). Although the O^+ signals detected by the probe laser from CO photodissociation at 193 nm were extremely weak, in a supersonic expansion of an 8% mixture of CO in argon, there was an apparent ~10% increase in the $J = 2$ sublevel within experimental error. At present, it is difficult to distinguish differences in the distributions which arise from the photodissociation of CO or CO-Ar (or higher order) van der Waals complexes.

There also may be dissociation wavelength effects in the nascent spin-orbit distributions. Miyawaki et al. (1990) have investigated the spin-orbit state distribution of oxygen $2p^4$ ($^3P_{2,1,0}$) produced in the photodissociation of NO_2 at four different wavelengths. They also report the propensity for the J = 2 level to be more populated than the high temperature limit. The distributions which were produced by 355- , 337- , and 266-nm photodissociations at 212 nm through a different electronic state yielded a different nascent state distribution. We decided to investigate the photodissociation of CO at another excimer laser wavelength (KrF at 248 nm) and observed signals from the photoproduction of CO^+. O^+ signals which we observed in pump-probe experiments were very weak, and, in addition, it was difficult to discern what fraction of atomic oxygen $2p^4$ ($^3P_{2,1,0}$) was produced from the dissociation of CO or CO^+ at this wavelength. We hope, in the future work, to extend this work using both a high resolution line tunable ArF excimer laser which can excite individual rotational lines of the spin-forbidden CO $a^3\Pi$, $v' = 2 \leftarrow X^1\Sigma^+$, $v'' = 0$ one-photon transitions and probe laser with subdoppler resolution to resolve upper state splittings of the fine structure components of atomic oxygen $2p^3 3p(^3P_{2,1,0})$.

4. CONCLUSION

The photodissociation of carbon monoxide at 193 nm has been investigated using REMPI detection of oxygen and carbon atoms under collision-free conditions. These new results are in excellent agreement with our previous experimental investigations which used oxygen-atom two-photon laser-induced fluorescence and suggest a quadratic photodissociation process in CO at 12.8 eV. The nascent fine structure branching ratios of atomic oxygen $2p^4(^3P_{2,1,0})$ from 193-nm photodissociation of CO are reported using oxygen (2+1) REMPI and two-photon laser-induced fluorescence and indicate that the distribution is not statistical. The experimental data were fit to a distribution which would correspond to a thermal temperature of 1,100 ±200 K.

At present, however, although predissociative processes appear to dominate the photoabsorption in this energy region, the precise identity of the dissociative state(s) is not entirely certain. Essentially, there is little known about the dependence of the branching ratios on the dissociation pathway (i.e., excitation wavelength, nonadiabatic, and spin-orbit coupling between dissociating states, curve crossings, and exit channel mixing effects).

5. REFERENCES

Bamford, D. J., L. E. Jusinski, and W. K. Bischel. Phys. Rev. A, vol. 34, p. 185, 1986.

Bischel, W. K., B. E. Perry, and D. R. Crosley. Phys. Rev. A, vol. 30, p. 1546, 1984.

Bokor, J., J. Zavelovich, and C. K. Rhodes. Journal of Chemical Physics, vol. 72, p. 965, 1980.

Buck, J. D., D. H. Parker, and D. W. Chandler. Journal of Physical Chemistry, vol. 92, p. 3701, 1988.

Cooper, D. M., and K. Kirby. Journal of Chemical Physics, vol. 74, p. 1200, 1981.

Cooper, D. M., and S. R. Langhoff. Journal of Chemical Physics, vol. 74, p. 1200, 1981.

Downey, S. W., and R. S. Hozack. Opt. Lett., vol. 14, p. 15, 1989.

Fock, J. -H., P. Gurtler, and E. E. Koch. Journal of Chemical Physics, vol. 47, p. 87, 1980.

Forch, B. E., K. T. Chen, H. Saigusa, and E. C. Lim. Journal of Physical Chemistry, vol. 87, p. 2280, 1983.

Forch, B. E., and E. C. Lim. Chemical Physics Letters, vol. 110, p. 593, 1984.

Hill, W. T., B. P. Turner, H. Lefebvre-Brion, S. Tang, and J. Zhu. Journal of Chemical Physics, vol. 92, p. 4272, 1990.

Huang, Y., and R. J. Gordon. Journal of Chemical Physics, vol. 93, p. 868, 1990.

Huang, Y., and R. J. Gordon. Journal of Chemical Physics, Submitted for publication.

Huber, K. P., and G. Herzberg. Molecular Spectra and Molecular Structure Vol. 4, Constants of Diatomic Molecules, New York: Van Nostrand Reinhold, 1979.

Krupenie, P. H. "The Bank Spectrum of Carbon Monoxide." National Standard Ref. Data Ser., vol. 5, National Bureau of Standards, 1966.

Laufer, G., R. L. McKenzie, and W. M. Huo. Opt. Lett., vol. 13, p. 99, 1988.

Lee, S., and K. F. Freed Journal of Chemical Physics, vol. 93, p. 868, 1990.

Letzelter, C., M. Eidelsberg, F. Rostas, J. Brenton, and B. Thielblemont. Journal of Chemical Physics, vol. 114, p. 273, 1987.

Lubman, D. L., and R. M. Jordan. Rev. Sci. Instrum., vol. 56, p. 373, 1985.

Matsumi, Y., and Masahiro Kawasaki. Journal of Chemical Physics, vol. 93, p. 2481, 1990.

Meijer, G., A. M. Wodtke, H. Voges, H. Schluter, and P. Andersen. Journal of Chemical Physics, vol. 89, p. 258, 1988.

Merrow, C. N., and B. E. Forch. Journal of Chemical Physics, vol. 93, p. 4791, 1990.

Miyawaki, J., T. Tsuchizawa, K. Yamanouchi, and S. Tsuchiya. Chemical Physics Letters, vol. 165, p. 168, 1990.

O'Neil, S. V., and H. F. Schaefer III. Journal of Chemical Physics, vol. 53, p. 3994, 1970.

Saigusa, H., B. E. Forch, and E. C. Lim. Journal of Chemical Physics, vol. 78, p. 2795, 1983.

Sausa, R. C., A. J. Alfano, and A. W. Miziolek. Applied Optics, vol. 26, p. 3588, 1987.

Sekine, S., Y. Adachi, and C. Hirose. Journal of Chemical Physics, vol. 90, p. 5346, 1989.

Vidal, C. R. Advances in Atomic and Molecular Physics. Edited by D. Bates and B. Bederson Boston: Academic, p. 1 (and references therein), 1988.

Yoshino, K., D. E. Freeman, and W. H. Parkinson. Journal of Physical Chemistry Ref. Data, vol. 13, p. 207, 1984.

No. of Copies	Organization
2	Administrator Defense Technical Info Center ATTN: DTIC-DDA Cameron Station Alexandria, VA 22304-6145
1	Commander U.S. Army Materiel Command ATTN: AMCAM 5001 Eisenhower Ave. Alexandria, VA 22333-0001
1	Commander U.S. Army Laboratory Command ATTN: AMSLC-DL 2800 Powder Mill Rd. Adelphi, MD 20783-1145
2	Commander U.S. Army Armament Research, Development, and Engineering Center ATTN: SMCAR-IMI-I Picatinny Arsenal, NJ 07806-5000
2	Commander U.S. Army Armament Research, Development, and Engineering Center ATTN: SMCAR-TDC Picatinny Arsenal, NJ 07806-5000
1	Director Benet Weapons Laboratory U.S. Army Armament Research, Development, and Engineering Center ATTN: SMCAR-CCB-TL Watervliet, NY 12189-4050
(Unclass. only)1	Commander U.S. Army Rock Island Arsenal ATTN: SMCRI-TL/Technical Library Rock Island, IL 61299-5000
1	Director U.S. Army Aviation Research and Technology Activity ATTN: SAVRT-R (Library) M/S 219-3 Ames Research Center Moffett Field, CA 94035-1000
1	Commander U.S. Army Missile Command ATTN: AMSMI-RD-CS-R (DOC) Redstone Arsenal, AL 35898-5010

No. of Copies	Organization
1	Commander U.S. Army Tank-Automotive Command ATTN: ASQNC-TAC-DIT (Technical Information Center) Warren, MI 48397-5000
1	Director U.S. Army TRADOC Analysis Command ATTN: ATRC-WSR White Sands Missile Range, NM 88002-5502
1	Commandant U.S. Army Field Artillery School ATTN: ATSF-CSI Ft. Sill, OK 73503-5000
2	Commandant U.S. Army Infantry School ATTN: ATZB-SC, System Safety Fort Benning, GA 31903-5000
(Class. only)1	Commandant U.S. Army Infantry School ATTN: ATSH-CD (Security Mgr.) Fort Benning, GA 31905-5660
(Unclass. only)1	Commandant U.S. Army Infantry School ATTN: ATSH-CD-CSO-OR Fort Benning, GA 31905-5660
1	WL/MNOI Eglin AFB, FL 32542-5000
	Aberdeen Proving Ground
2	Dir, USAMSAA ATTN: AMXSY-D AMXSY-MP, H. Cohen
1	Cdr, USATECOM ATTN: AMSTE-TC
3	Cdr, CRDEC, AMCCOM ATTN: SMCCR-RSP-A SMCCR-MU SMCCR-MSI
1	Dir, VLAMO ATTN: AMSLC-VL-D
10	Dir, USABRL ATTN: SLCBR-DD-T

No. of Copies	Organization
1	HQDA (SARD-TC, C.H. Church) WASH DC 20310-0103
4	Commander US Army Research Office ATTN: R. Ghirardelli D. Mann R. Singleton R. Shaw P.O. Box 12211 Research Triangle Park, NC 27709-2211
2	Commander US Army Armament Research, Development, and Engineering Center ATTN: SMCAR-AEE-B, D.S. Downs SMCAR-AEE, J.A. Lannon Picatinny Arsenal, NJ 07806-5000
1	Commander US Army Armament Research, Development, and Engineering Center ATTN: SMCAR-AEE-BR, L. Harris Picatinny Arsenal, NJ 07806-5000
2	Commander US Army Missile Command ATTN: AMSMI-RD-PR-E, A.R. Maykut AMSMI-RD-PR-P, R. Betts Redstone Arsenal, AL 35898-5249
1	Office of Naval Research Department of the Navy ATTN: R.S. Miller, Code 432 800 N. Quincy Street Arlington, VA 22217
1	Commander Naval Air Systems Command ATTN: J. Ramnarace, AIR-54111C Washington, DC 20360
1	Commander Naval Surface Warfare Center ATTN: J.L. East, Jr., G-23 Dahlgren, VA 22448-5000

No. of Copies	Organization
2	Commander Naval Surface Warfare Center ATTN: R. Bernecker, R-13 G.B. Wilmot, R-16 Silver Spring, MD 20903-5000
5	Commander Naval Research Laboratory ATTN: M.C. Lin J. McDonald E. Oran J. Shnur R.J. Doyle, Code 6110 Washington, DC 20375
1	Commanding Officer Naval Underwater Systems Center Weapons Dept. ATTN: R.S. Lazar/Code 36301 Newport, RI 02840
2	Commander Naval Weapons Center ATTN: T. Boggs, Code 388 T. Parr, Code 3895 China Lake, CA 93555-6001
1	Superintendent Naval Postgraduate School Dept. of Aeronautics ATTN: D.W. Netzer Monterey, CA 93940
3	AL/LSCF ATTN: R. Corley R. Geisler J. Levine Edwards AFB, CA 93523-5000
1	AFOSR ATTN: J.M. Tishkoff Bolling Air Force Base Washington, DC 20332
1	OSD/SDIO/IST ATTN: L. Caveny Pentagon Washington, DC 20301-7100

No. of
Copies Organization

1 Commandant
USAFAS
ATTN: ATSF-TSM-CN
Fort Sill, OK 73503-5600

1 F.J. Seiler
ATTN: S.A. Shackleford
USAF Academy, CO 80840-6528

1 University of Dayton Research Institute
ATTN: D. Campbell
AL/PAP
Edwards AFB, CA 93523

1 NASA
Langley Research Center
Langley Station
ATTN: G.B. Northam/MS 168
Hampton, VA 23365

4 National Bureau of Standards
ATTN: J. Hastie
M. Jacox
T. Kashiwagi
H. Semerjian
US Department of Commerce
Washington, DC 20234

1 Aerojet Solid Propulsion Co.
ATTN: P. Micheli
Sacramento, GA 95813

1 Applied Combustion Technology, Inc.
ATTN: A.M. Varney
P.O. Box 607885
Orlando, FL 32860

2 Applied Mechanics Reviews
The American Society of
Mechanical Engineers
ATTN: R.E. White
A.B. Wenzel
345 E. 47th Street
New York, NY 10017

1 Atlantic Research Corp.
ATTN: R.H.W. Waesche
7511 Wellington Road
Gainesville, VA 22065

No. of
Copies Organization

1 AVCO Everett Research
Laboratory Division
ATTN: D. Stickler
2385 Revere Beach Parkway
Everett, MA 02149

1 Battelle
ATTN: TACTEC Library, J. Huggins
505 King Avenue
Columbus, OH 43201-2693

1 Cohen Professional Services
ATTN: N.S. Cohen
141 Channing Street
Redlands, CA 92373

1 Exxon Research & Eng. Co.
ATTN: A. Dean
Route 22E
Annandale, NJ 08801

1 General Applied Science
Laboratories, Inc.
77 Raynor Avenue
Ronkonkama, NY 11779-6649

1 General Electric Ordnance
Systems
ATTN: J. Mandzy
100 Plastics Avenue
Pittsfield, MA 01203

1 General Motors Rsch Labs
Physical Chemistry Department
ATTN: T. Sloane
Warren, MI 48090-9055

2 Hercules, Inc.
Allegheny Ballistics Lab.
ATTN: W.B. Walkup
E.A. Yount
P.O. Box 210
Rocket Center, WV 26726

1 Alliant Techsystems, Inc.
Marine Systems Group
ATTN: D.E. Broden/
MS MN50-2000
600 2nd Street NE
Hopkins, MN 55343

No. of Copies	Organization
1	Alliant Techsystems, Inc. ATTN: R.E. Tompkins MN38-3300 5700 Smetana Drive Minnetonka, MN 55343
1	IBM Corporation ATTN: A.C. Tam Research Division 5600 Cottle Road San Jose, CA 95193
1	IIT Research Institute ATTN: R.F. Remaly 10 West 35th Street Chicago, IL 60616
2	Director Lawrence Livermore National Laboratory ATTN: C. Westbrook M. Costantino P.O. Box 808 Livermore, CA 94550
1	Lockheed Missiles & Space Co. ATTN: George Lo 3251 Hanover Street Dept. 52-35/B204/2 Palo Alto, CA 94304
1	Director Los Alamos National Lab ATTN: B. Nichols, T7, MS-B284 P.O. Box 1663 Los Alamos, NM 87545
1	National Science Foundation ATTN: A.B. Harvey Washington, DC 20550
1	Olin Ordnance ATTN: V McDonald, Library P.O. Box 222 St. Marks, FL 32355-0222
1	Paul Gough Associates, Inc. ATTN: P.S. Gough 1048 South Street Portsmouth, NH 03801-5423

No. of Copies	Organization
2	Princeton Combustion Research Laboratories, Inc. ATTN: M. Summerfield N.A. Messina 475 US Highway One Monmouth Junction, NJ 08852
1	Hughes Aircraft Company ATTN: T.E. Ward 8433 Fallbrook Avenue Canoga Park, CA 91303
1	Rockwell International Corp. Rocketdyne Division ATTN: J.E. Flanagan/HB02 6633 Canoga Avenue Canoga Park, CA 91304
4	Director Sandia National Laboratories Division 8354 ATTN: R. Cattolica S. Johnston P. Mattern D. Stephenson Livermore, CA 94550
1	Science Applications, Inc. ATTN: R.B. Edelman 23146 Cumorah Crest Woodland Hills, CA 91364
3	SRI International ATTN: G. Smith D. Crosley D. Golden 333 Ravenswood Avenue Menlo Park, CA 94025
1	Stevens Institute of Tech. Davidson Laboratory ATTN: R. McAlevy, III Hoboken, NJ 07030
1	Sverdrup Technology, Inc. LERC Group ATTN: R.J. Locke, MS SVR-2 2001 Aerospace Parkway Brook Park, OH 44142

No. of Copies | Organization

1 Sverdrup Technology, Inc.
ATTN: J. Deur
2001 Aerospace Parkway
Brook Park, OH 44142

1 Thiokol Corporation
Elkton Division
ATTN: S.F. Palopoli
P.O. Box 241
Elkton, MD 21921

3 Thiokol Corporation
Wasatch Division
ATTN: S.J. Bennett
P.O. Box 524
Brigham City, UT 84302

1 United Technologies Research Center
ATTN: A.C. Eckbreth
East Hartford, CT 06108

3 United Technologies Corp.
Chemical Systems Division
ATTN: R.S. Brown
T.D. Myers (2 copies)
P.O. Box 49028
San Jose, CA 95161-9028

1 Universal Propulsion Company
ATTN: H.J. McSpadden
Black Canyon Stage 1
Box 1140
Phoenix, AZ 85029

1 Veritay Technology, Inc.
ATTN: E.B. Fisher
4845 Millersport Highway
P.O. Box 305
East Amherst, NY 14051-0305

1 Brigham Young University
Dept. of Chemical Engineering
ATTN: M.W. Beckstead
Provo, UT 84058

1 California Institute of Tech.
Jet Propulsion Laboratory
ATTN: L. Strand/MS 512/102
4800 Oak Grove Drive
Pasadena, CA 91109

No. of Copies | Organization

1 California Institute of Technology
ATTN: F.E.C. Culick/MC 301-46
204 Karman Lab.
Pasadena, CA 91125

1 University of California
Los Alamos Scientific Lab.
P.O. Box 1663, Mail Stop B216
Los Alamos, NM 87545

1 University of California, Berkeley
Chemistry Deparment
ATTN: C. Bradley Moore
211 Lewis Hall
Berkeley, CA 94720

1 University of California, San Diego
ATTN: F.A. Williams
AMES, B010
La Jolla, CA 92093

2 University of California, Santa Barbara
Quantum Institute
ATTN: K. Schofield
M. Steinberg
Santa Barbara, CA 93106

1 University of Colorado at Boulder
Engineering Center
ATTN: J. Daily
Campus Box 427
Boulder, CO 80309-0427

2 University of Southern California
Dept. of Chemistry
ATTN: S. Benson
C. Wittig
Los Angeles, CA 90007

1 Cornell University
Department of Chemistry
ATTN: T.A. Cool
Baker Laboratory
Ithaca, NY 14853

No. of Copies | Organization

1 University of Delaware
ATTN: T. Brill
Chemistry Department
Newark, DE 19711

1 University of Florida
Dept. of Chemistry
ATTN: J. Winefordner
Gainesville, FL 32611

3 Georgia Institute of Technology
School of Aerospace Engineering
ATTN: E. Price
W.C. Strahle
B.T. Zinn
Atlanta, GA 30332

1 University of Illinois
Dept. of Mech. Eng.
ATTN: H. Krier
144MEB, 1206 W. Green St.
Urbana, IL 61801

1 Johns Hopkins University/APL
Chemical Propulsion
Information Agency
ATTN: T.W. Christian
Johns Hopkins Road
Laurel, MD 20707

1 University of Michigan
Gas Dynamics Lab
Aerospace Engineering Bldg.
ATTN: G.M. Faeth
Ann Arbor, MI 48109-2140

1 University of Minnesota
Dept. of Mechanical
Engineering
ATTN: E. Fletcher
Minneapolis, MN 55455

3 Pennsylvania State University
Applied Research Laboratory
ATTN: K.K. Kuo
H. Palmer
M. Micci
University Park, PA 16802

No. of Copies | Organization

1 Pennsylvania State University
Dept. of Mechanical Engineering
ATTN: V. Yang
University Park, PA 16802

1 Polytechnic Institute of NY
Graduate Center
ATTN: S. Lederman
Route 110
Farmingdale, NY 11735

2 Princeton University
Forrestal Campus Library
ATTN: K. Brezinsky
I. Glassman
P.O. Box 710
Princeton, NJ 08540

1 Purdue University
School of Aeronautics
and Astronautics
ATTN: J.R. Osborn
Grissom Hall
West Lafayette, IN 47906

1 Purdue University
Department of Chemistry
ATTN: E. Grant
West Lafayette, IN 47906

2 Purdue University
School of Mechanical
Engineering
ATTN: N.M. Laurendeau
S.N.B. Murthy
TSPC Chaffee Hall
West Lafayette, IN 47906

1 Rensselaer Polytechnic Inst.
Dept. of Chemical Engineering
ATTN: A. Fontijn
Troy, NY 12181

1 Stanford University
Dept. of Mechanical
Engineering
ATTN: R. Hanson
Stanford, CA 94305

No. of Copies	Organization
1	University of Texas Dept. of Chemistry ATTN: W. Gardiner Austin, TX 78712
1	University of Utah Dept. of Chemical Engineering ATTN: G. Flandro Salt Lake City, UT 84112
1	Virginia Polytechnic Institute and State University ATTN: J.A. Schetz Blacksburg, VA 24061
1	Freedman Associates ATTN: E. Freedman 2411 Diana Road Baltimore, MD 21209-1525

INTENTIONALLY LEFT BLANK.